Available online at www.sciencedirect.com
ScienceDirect
Journal of Nuclear Materials 377 (2008) 253–260
journal of nuclear materials
www.elsevier.com/locate/jnucmat

Liquid metal embrittlement of T91 and 316L steels by heavy liquid metals: A fracture mechanics assessment

T. Auger *, Z. Hamouche, L. Medina-Almazàn, D. Gorse

CNRS, CECM, UPR2801, 15 rue Georges Urbain, 94407 Vitry sur Seine, France

Abstract

LME of the martensitic T91 and the austenitic 316L steels have been investigated in the CCT geometry in the plane-stress condition. Using such a geometry, premature cracking induced by a liquid metal (PbBi and Hg) can be studied using a fracture mechanics approach based on CTOD, J–Δa and fracture assessment diagram. One is able to measure a reduction of the crack tip blunting and a reduction of the energy required for crack propagation induced by the liquid metal. In spite of some limitations, this qualitative evaluation shows that liquid metals do not induce strong embrittlement on steels in plane-stress condition. Rather, the effect of the liquid metal seems to promote a fracture mode by plastic collapse linked with strain localization. It indicates that the materials, in spite of a potential embrittlement, should still be acceptable in terms of safety criteria.

1. Introduction

The martensitic T91 and the austenitic 316L steels are the two selected structural materials for neutron sources based on spallation targets built so far: MEGAPIE at the Paul Scherrer Institute (PSI) and the Spallation Neutron Source at ORNL (Oak Ridge National Lab.) [1,2]. The heavy liquid metals used in these systems are mercury (Hg) and Lead–Bismuth eutectic (LBE) alloy. In the standard metallurgical condition, these two materials show a susceptibility to liquid metal embrittlement (LME) provided the liquid metal is in intimate contact with the material and also that large plastic deformation takes place [3,4]. One of the key parameters of this phenomenon is wetting. It is one of the experimental difficulties that have precluded serious investigation so far. The native oxides of steels, particularly those composed of chromium oxide, are not wetted by liquid metals and are very stable in reducing environment. In such case, there is no contact between the material and the liquid metal and there is no change in the plastic deformation mode. It has therefore been of the utmost difficulty to be able to study in a reproducible way the phenomenon until pre-wetting procedures of mechanical testing specimen were developed [5].

The observed rupture mode can be either quasi-cleavage (crack opening in mode I) or shear and tear decohesion (crack opening in modes II–III). Brittle fracture as well as plastic collapse can both be observed. The rupture is to be classified as a special case of quasi-brittle environmental rupture with the peculiarity that the damage mechanism occurs at the surface. Although in the case of steels, liquid metal induced cracking is preceded by considerable prior plastic deformation, the assessment of the risk of liquid metal induced embrittlement (LMIE) is still required for licensing and confidence in safe operation of spallation targets. Fracture mechanics is therefore required to assess the degree of embrittlement induced by the liquid metal.

Standard fracture mechanics approach is not well suited for direct applicability. The main problem lies in the fact that wetting at the crack tip must absolutely be ensured for any measurement to be meaningful and reproducible. The pre-cracking procedure by fatigue recommended in ASTM-1820 discards any further attempt to control that fundamental parameter. There is no experimental means

* Corresponding author. Tel.: +33 (0) 1 41 13 10 00; fax: +33 (0) 1 41 13 14 30.
E-mail address: thierry.auger@ecp.fr (T. Auger).

0022-3115/$ - see front matter © 2008 Elsevier B.V. All rights reserved.
doi:10.1016/j.jnucmat.2008.02.043

up to now allowing a controlled removal of the native oxide that spontaneously forms on crack walls. Since this nanometer thick native oxide usually prevents wetting by liquid metals, the liquid metal cannot reach the crack tip. Due to the confined geometry of a crack opening, long term exposure of a pre-cracked specimen does not even ensure that the liquid metal will fill the opening up to the crack tip. In the work reported in this paper, a procedure allowing wetting to be achieved at the notch root is used at the price that pre-cracking is not performed. Instead, premature cracking is indeed induced by the liquid metal.

In order to explore and quantify the damage induced by liquid metals, we developed a fracture mechanics test based on center cracked in tension (CCT) specimen. Spallation sources use thin sheets and thin tubes of structural material. It is also needed to develop modified test procedures that closely reproduce in-service plane-stress conditions. This paper is one step towards this goal. The crack propagation process is studied in thin sheets of materials by the crack tip opening displacement (CTOD) approach and J–Δa curve measurement. Failure assessment diagram are also constructed from the J data.

2. Fracture mechanics

2.1. Experiments

Crack length measurement is required to quantify crack growth dynamics. Liquid metals are conductive and opaque media. This precludes the use of standard crack growth monitoring methods such as the potential drop method because the liquid metal short-circuits the current path. The compliance method is not suitable due to scattering in the amount of uniform elongation before cracking and strain localization. It is therefore difficult to uniquely estimate by finite-element the relationship between crack length and the compliance. The method used in this work is the visual recording of the specimen taking advantage of a test apparatus especially designed for this purpose. The CCT geometry with a centered notch (2.5 mm height, 10 mm length, notch root radius of ≈0.3 mm – Fig. 1(a)) provides enough space to be filled by the liquid metal. Due to the reduced amount of liquid metal used in each test (≈1/10th of a cm^3) surface tension and a wetting condition is strong enough to counter the fall of the liquid metal by gravity. However, in order to be able to manipulate the wetted specimen, a transparent quartz foil was mechanically maintained along the sides of the specimen. This also prevented the fall of liquid metal into the apparatus while dismantling the specimen after testing.

When the crack opens, capillarity driven flow supplies the liquid metal at the crack tip. This is a key point: wetting by the liquid metal is ensured within the notch prior to initial cracking by chemical fluxing. With such setup, there is no surrounding liquid metal to prevent from visual recording. With thin sheets of materials in plane-stress condition, the crack growth monitoring can be reduced to monitoring the crack length in one dimension with a relatively low uncertainty. A CCD camera system records the crack length during the experiment (Fig. 1(b)). Since the surface of the liquid metal appears bright and mirror like, the crack tip location is taken at the edge of the farthest liquid metal area intersecting with the mat aspect of the steel surface. The crack growth rate is then equated from the visual recording to the crack tip speed.

Heating of the sample can be performed by the internal heating method (Joule effect of the specimen itself). A high intensity/low voltage current flows through the specimen using a ground isolated loop. The temperature is measured by a near infrared pyrometer ahead of the crack tip. A feedback loop regulates the temperature by a PID algorithm actuating the power injection through a thyristor. Additionally, we checked by using an near infrared camera (measuring at the 0.9 μm wavelength equipped with a Kodak 87C filter for photography) that the temperature field is homogeneous along the width of the sample. With this heating technique, there is a temperature gradient only along the length of the specimen towards the grips that are heat sinks (Fig. 1(c)). The whole experimental setup including the grips is under flowing He–4%H_2 cover gas to prevent from oxidation. A transparent quartz tube containing the whole setup is used for isolation from air. The quartz is made of a special anhydrous type to avoid strong absorption in the 1.4–1.6 μm waveband so that the temperature measurement by pyrometry is almost not affected. The oxygen content of the flowing gas is monitored using a stabilized zirconia oxygen probe (SETNAG© oxygen probe). It is usually very low and prevents the sample and the liquid metal from oxidation in the course of an experiment.

No pre-cracking is performed in order to be able to ensure crack tip wetting by the liquid metal. Instead, the center notch is wetted by a dedicated chemical fluxing procedure prior to mounting into the test machine [5]. The operating conditions (strain rate and temperature) are chosen so that the liquid metal induces initial cracking in a brittle manner.

Tensile loading is performed on an MTS 20/MH tensile machine. The loading sequence is to load the sample for 30–60 s duration at constant cross-head displacement rate (0.04 mm/min). Then the specimen is unloaded of 10% of the maximum load reached during the loading sequence. The crack length is then measured optically and the overall sequence repeated until one of the two cracks reaches the edge of the sample. Then the experiment is stopped and eventually cooled down. The force and displacement is recorded during the experiment and correlated with the crack length at any time in the post-test analysis.

2.2. Materials

The composition of the steels is reported in the Table 1. Two materials/liquid metal combinations have been used: the 316L austenitic steel in contact with Hg and the martensitic steel T91 in contact with the eutectic PbBi alloy.

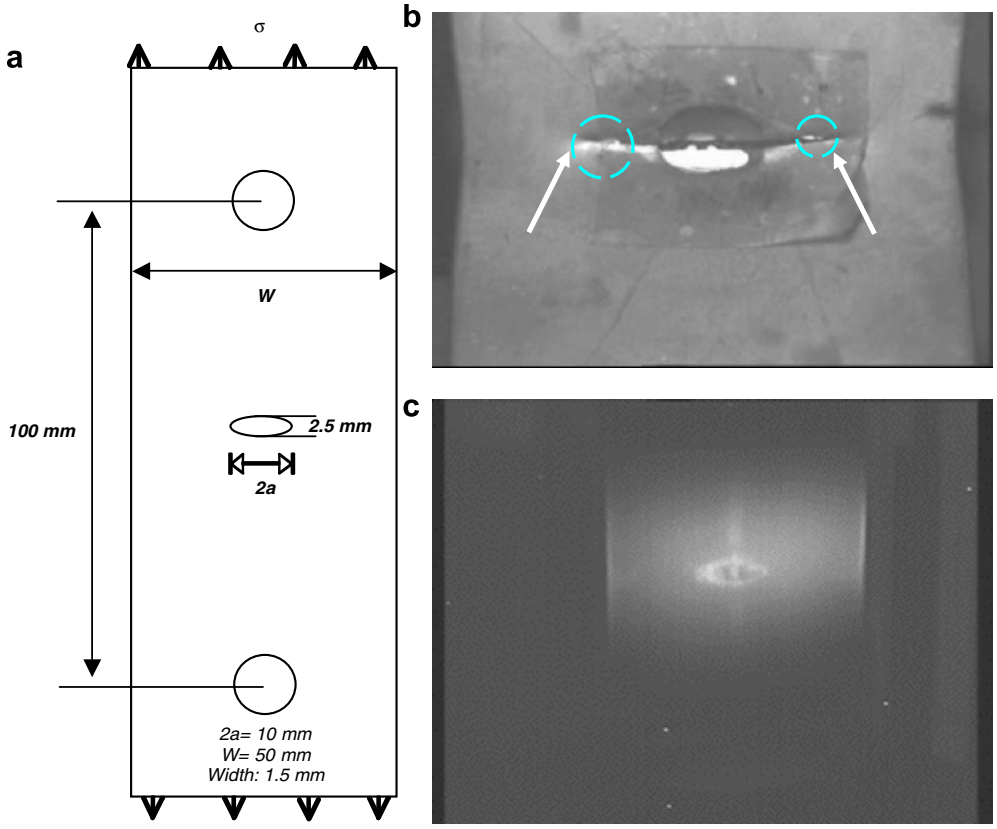

Fig. 1. (a) Schematic of the samples used for fracture mechanics testing (1.5 mm thickness). (b) Image extracted from a video of 316L SS CCT specimen tested in mercury at 6.67×10^{-5} cm s^{-1} deformation rate. Hg is observed at the crack tip on both sides of the specimen as indicated by the circled areas. (c) Infrared image showing a qualitative view of the temperature field in the CCT geometry (no temperature scale is available).

Table 1
Composition of austenitic 316L and martensitic T91 steels

Steel	C	Si	Mn	P	S	Cr	Mo	Ni	Al	Cu	Nb	Ti	V
316L	0.0185	0.67	1.81	0.032	0.0035	16.73	2.05	9.97	0.0183	0.23	–	0.0058	0.07
T91	0.1025	0.22	0.38	0.021	0.0004	8.99	0.89	0.11	0.0146	0.06	0.06	0.0034	0.21

Reference measurements were also performed with both steels and are used for comparison with the standard ductile fracture. The embrittlement effect on 316L and T91 steels has been reproduced many times and at different cross-head speeds [4]. The fracture mechanics assessment has been performed with one experiment for each of the 316L/Hg and T91/LBE combination.

The 316L austenitic steel is in the annealed metallurgical condition. The T91 martensitic steel is in the standard condition, austenitized at 1050 °C for 1 h followed by water quenching, then tempered for 1 h at 750 °C followed by air cooling. The specimens available as sheets of 1.5 mm were machined according to the schematic presented in Fig. 1(a).

2.3. Results: CTOD

In this study, although extensive plastic deformation occurred prior to fracture, linear elastic fracture mechanics concepts are used in order to derive qualitative mechanical information on the embrittlement effect ahead of crack tip. The crack tip opening displacement (CTOD, δ_{CTT}) is obtained from the crack tip mouth displacement (CTMD, Δ) measurement. The center of hinge is visually determined by the rotational factor analysis. For plane-stress conditions, the crack tip opening displacement is given by

$$\delta_{CTT}(a) \approx \frac{K^2(a)}{\sigma_{ys}(a) \cdot E}.$$

A simple parameterization of the stress intensity factor K for a plate of width w loaded in tension with a centrally located crack of length $2a$ is used [6]. The stress component of K is approximated by an equivalent stress computed taking into account the reduction of area generated by the plastic deformation prior to crack initiation. The width used in the calculation of the stress is indeed measured by SEM on the rupture profile (Fig. 2(a)). One interrupted test was performed on 316L with Hg to reveal the inner crack geometry (Fig. 2(b)). The Hg was then removed by exposing the sample covered with water to an ultrasonic

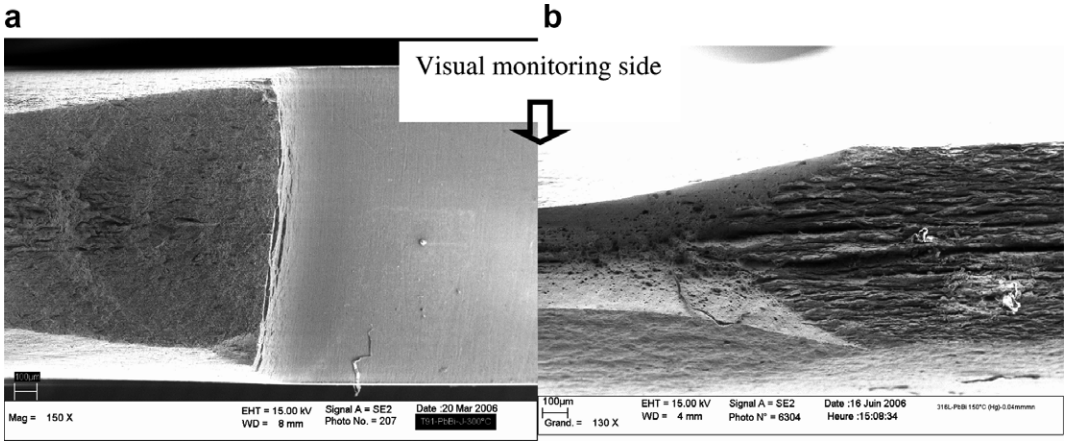

Fig. 2. (a) SEM top view of the crack initiation site in a T91-PbBi experiment at 300 °C (crack propagation is vertical). (b) SEM view of the crack tip at the transition area obtained from a crack arrest experiment of 316L–Hg (crack propagation runs from the right to the left).

cleaning device for one minute. After removal of the Hg, the sample was completely broken to reveal the crack tip geometry (Fig. 2(b)). One can notice the tunneling effect induced by the liquid metal which results in the crack being further advanced at the center than on the edges. Because of this tunneling effect, the length measured from the surface crack is less than the length of the inner part of the real crack. However this systematic error represents only a few hundreds μm and it is neglected in the present work.

Since δ_{CTT} and K are independently measured, the effect of the liquid metal can be evaluated by using the small scale yielding stress evolution $\sigma_{ys}(a)$ as an indicator of the degree of work hardening reached before cracking. This is particularly well suited for 316L because in that case, the small scale yielding stress extracted from the CTOD allows for a clear discrimination between the ductile and brittle fracture. In the CCT geometry, in the absence of mercury, the tensile component of the stress tensor produces strain hardening ahead of the crack tip as the crack advances. On the opposite, the contact of the crack tip with Hg induces a net decrease of the strain hardening as measured by the estimated crack tip yield stress since it saturates at a lower value (Fig. 3(a)). This reflects the fact that extended plastic deformation does not occur when Hg is present at the crack tip. Crack tip blunting is clearly impaired or in other word, the plastic flow is localized at the crack tip.

In the case of T91 in contact with the eutectic PbBi (here presented from results obtained at 160 °C), the effect on the measured crack tip opening is also clearly seen (Fig. 3(b)). In the case of a ductile rupture, blunting at the crack tip leads to a CTOD that increases rapidly up to the point where extended shear band plastic deformation prevents any further analysis. In the case of a contact with PbBi, the CTOD saturates at a lower value and remains nearly constant as the crack propagates. Furthermore, stable crack growth extends to very large crack size for the CCT geometry before extended plastic deformation by shear band proceeds (up to $a/w \approx 0.7$). This large decrease in the CTOD reflects the fact that the liquid metal promotes faster crack growth and prevents to a large extend crack tip blunting. Here again, the liquid metal induces plastic flow localization at the crack tip.

In spite of the striking difference in this mechanical analysis between ductile and brittle behavior, the CTOD

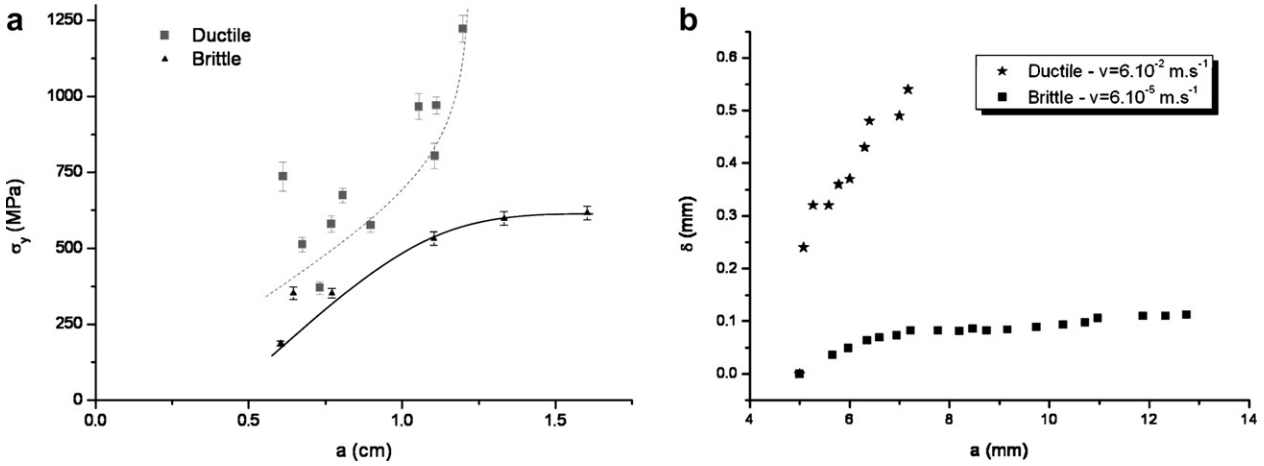

Fig. 3. Results of CTOD analysis (a) 316L–Hg at room temperature and (b) T91-PbBi at 160 °C.

analysis is of little help for engineering design. More quantitative results are given in the following section by the J–Δa technique.

2.4. Results: fracture resistance J–Δa measurement

The raw data used for the J analysis for 316L in contact with Hg are shown below (Fig. 4). Hg has a large effect on crack initiation. The onset of cracking is visible from the raw data as a sudden drop in the force–displacement record. Hg triggers early cracking compared to the case without Hg. Crack initiation occurs however after large plastic deformation. Astonishingly, the crack propagation is not so much affected because it requires a continuous supply of energy and the crack growth process is sub-critical. Furthermore, the energy spent in opening and propagating the crack is still very large. On average, the effect of Hg is to increase the crack propagation rate by a factor of 2.

As a first approximation, the fracture resistance J is evaluated by separating the elastic part and the plastic part [7]. J_0 related to the initial energy spent in opening the crack reads as

$$J_0 = \frac{K^2}{E} + \frac{U^*}{B(w-a_0)}.$$

Then each crack propagation is related to the incremental formulation of J as follows:

$$J_i = J_{i-1} + \frac{2\Delta U^*}{B(b_{j-1}+b_j)} + \frac{2}{E(b_{j-1}+b_j)}[K_j^2 b_j - K_{j-1}^2 b_{j-1}],$$

with $b = w - a$. The J–Δa curve obtained using this formula is shown in the Fig. 5 evaluated from the onset of cracking.

The evaluation of J is valid only up to $a = 0.4w$, crack extension data beyond that limit are not pictured on Fig. 5. One can notice a quadratic increase of the fracture resistance of 316L in air as the crack propagates. This reflects, as well as the CTOD analysis; the fact that the CCT geometry has a large tensile component (T stress). In the thin CCT geometry, extended plastic deformation ahead of the crack tip increases the energy required for propagating further the crack. Furthermore, the area of the sample under extended plastic deformation extends as the crack propagates giving a non linear increase to J. However, the fact that the small scale yielding condition is not fulfilled casts some doubts on the evaluation of J in the case of 316L alone because specimen size effects are large. On the opposite, in the presence of Hg, the nearly linear increase of J as the crack is propagated reflects the fact that the liquid metal induced cracking restricts plastic deformation mostly at the crack tip and that constant energy expenditure is required to propagate the crack. It indicates that there should be a rather strong strain localization that is induced by the liquid metal. Indeed, the CTOD is nearly constant during propagation confirming that plastic deformation is mostly restricted to the crack tip.

Similar analysis was carried out with T91. In that geometry, it is unfortunately not possible to reliably measure a full J–Δa reference curve for the T91 steel because extended shear band localization occurs almost after the crack initiation. This is an effect due to the CCT geometry in the thin plate used in conjunction with the martensitic material type where the work hardening rate is low. The beginning of the curve is only measurable up to $\Delta a \approx 1$ mm. Accordingly, the results are only presented up to that limit (see Fig. 6). In the case where T91 is in contact with PbBi, the shear band localization occurs at a later stage so that the test is

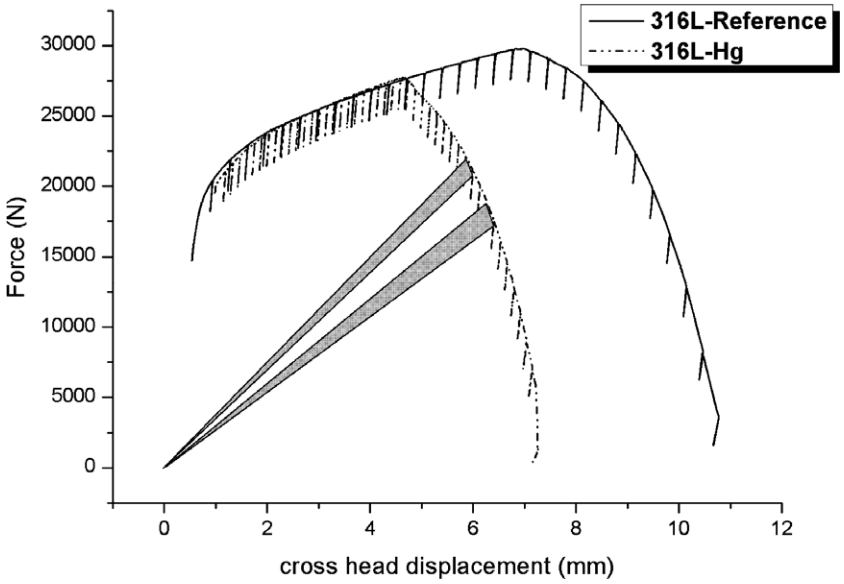

Fig. 4. 316L and 316L–Hg load–displacement curves. The shaded areas represent U^*.

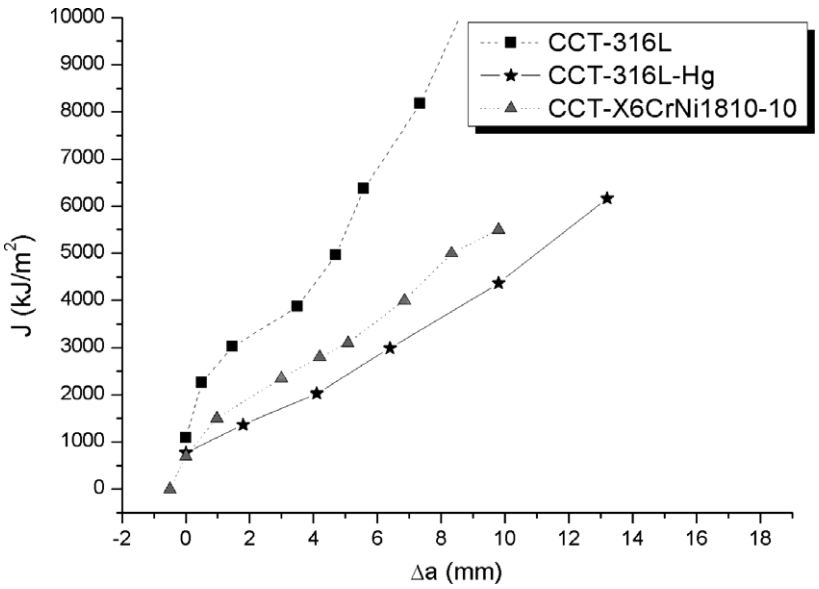

Fig. 5. J–Δa curve of 316L and 316L in contact with Hg at room temperature. A reference curve (10 mm thickness) for a similar austenitic steel is shown for comparison [8].

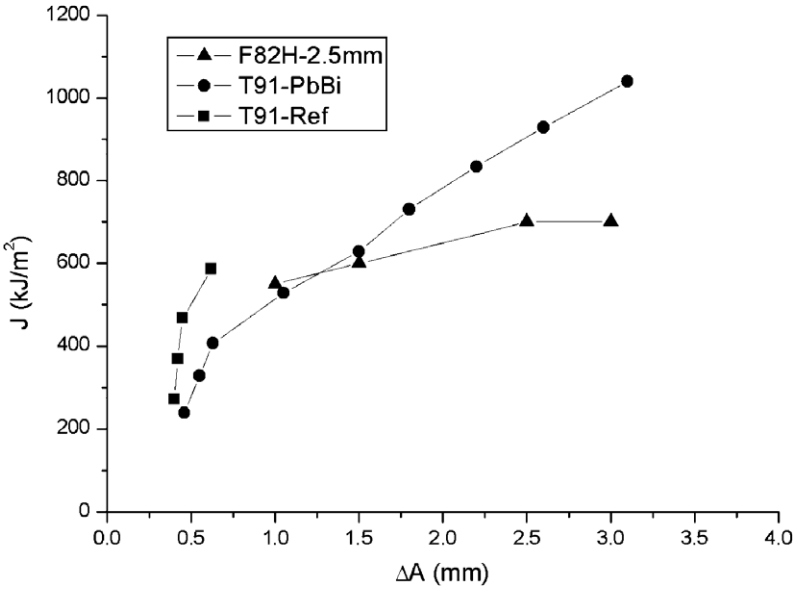

Fig. 6. J–Δa curve of T91 reference and T91 in contact with PbBi at 160 °C. The triangles represent the F82H reduced activation martensitic steel data with 2.5 mm thickness.

valid up to $\Delta a \approx 3$ mm. Beyond this point, for the same reason than for the reference T91, the measurement is no longer meaningful.

Extrapolating the J measurement of reference T91 to larger crack size would show a lowering of J when the T91 crack tip is in contact with PbBi compared to the reference case. Indeed, from the beginning of the J–Δa curves, one can notice a slight reduction of J. It is however difficult to quantify that reduction accurately since the difference could be due to the accuracy of the Δa measurement. For example using another set of data (not shown here) obtained with a specimen thickness of 1 mm, the difference is no longer visible. This result is at first sight, in striking contrast with the one obtained with 316L and Hg where a clear departure was clearly noticeable from the beginning. However the raw data (not shown here) indicate that crack growth requires less energy when PbBi is in contact with T91. One could also change the definition of the J used for building the J–Δa curve: by taking U instead of U^* [9], one would concentrate on the dJ/da measurement rather than the J–Δa curve.

Interestingly, a comparable measurement has been made on a CT specimen with a thickness of 2.5 mm for a similar type of steel, the reduced activation martensitic F82H steel [10] (see Fig. 6). This shows that the results in the CCT geometry are not impaired by a major flaw.

3. Fracture assessment diagram

Using the J–Δa analysis, one can build a fracture assessment diagram (FAD) which is a trajectory in the K_r and L_r parameter plane. This type of analysis is useful for the evaluation of the resistance of cracked component. It relies on the definition of 2 quantities describing the ratio between the applied load to the failure load (K_r) and the ratio between the applied load to the plastic collapse failure load (L_r).

$$K_r = \frac{\text{Applied Load}}{\text{Failure Load}} = \frac{K_1}{K_{1C}},$$

$$L_r = \frac{\text{Applied Load}}{\text{Plastic collapse failure load}} = \frac{\sigma}{\sigma_c}.$$

These above definitions are strictly valid for a brittle fracture in the elastic range or a ductile fracture up to the point of crack initiation. They have been modified to be applicable for an elasto-plastic fracture [11]. In this approach, the K_r and L_r parameters are defined from the J measurement and read as follows:

$$K_r = \sqrt{\frac{J_e}{J}} \quad \text{and} \quad L_r = \frac{\sigma}{\sigma_c(a/W)}.$$

The failure assessment line defines the boundary between stable and unstable crack growth behavior. Using the data from the J–Δa measurement, The results for 316L compared with 316L in contact with Hg are displayed on the Fig. 7.

One can see that the difference in trajectory is not large but still significantly different. Indeed a trajectory with K_r close to 1 would indicate a very brittle fracture in the linear elastic range. The trajectory in the (K_r, L_r) plane becomes a little closer to the brittle limiting case when Hg contact 316L. This indicates that the fracture process proceeds in a more 'brittle' manner than the typical ductile mode of 316L. This type of approach would certainly be valuable in order to discuss synergistic effects of irradiation and LME.

4. Discussion

The main result of this work is the establishment of an experimental procedure able to measure the effect of a liquid metal on the crack growth process from a fracture mechanics point of view. With some restrictions mostly due the small thickness of the samples, it has become possible to ascertain the LME effect in terms of several 'standard' fracture mechanics parameters: the CTOD, J–Δa curve and FAD. They have been shown to be potentially sensible indicators of the effect of a liquid metal on the fracture toughness. The main difficulty in such type of evaluation is the wetting of the crack tip by the liquid metal. It is shown here that by using thin plates in the CCT geometry, one is able to overcome it. The disadvantage is that one has to sacrifice meaningful absolute measurement due to the reduced thickness. It is also possible that the measurements have to be performed with several thicknesses to take into account specimen size effects.

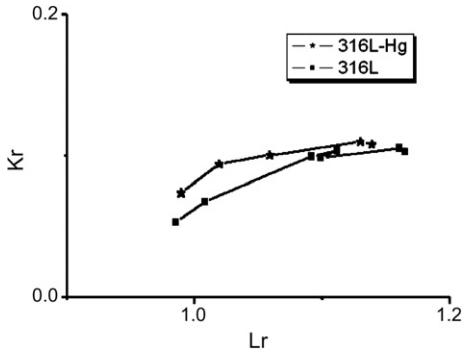

Fig. 7. FAD for 316L and 316L–Hg.

The CTOD analysis reveals very clearly that in both case (austenitic and martensitic steels) the liquid metal has a profound effect on the evolution of the crack growth and the crack geometry. Crack tip blunting is impaired by the liquid metal. It gives an important indication that an embrittlement process is taking place.

The J–Δa analysis of 316L in contact with Hg compared with 316L reveals the magnitude of the damage induced by Hg. The reduction in terms of energy density is at least of the order of a factor 2. This is large but not catastrophic from the design point of view. It is still compatible with a safe use of the material since safety margins in mechanical design should prevent large plastic deformation for structural material. Crack growth however clearly requires less energy by crack growth increase unit. In that respect, it corresponds to an embrittlement process in the sense that the fracture resistance is decreased. The martensitic T91 steel case is more complex to analyze: the energy required to propagate a crack seems to be affected by the liquid metal. However, as indicated previously, the crack propagation could not be followed on a sufficient length due to shear band flow localization. One can think that if the reference measurement could be performed with larger crack size, the J–Δa curve would be clearly lower in the case of a contact with a liquid metal. This is a restriction of the test geometry used here that it can be difficult to reliably evaluate reference curves. Surprisingly, in spite of the limitations afore mentioned, the J–Δa curves are in qualitative agreement compared with those obtained when available in the CCT geometry using thicker samples.

The fracture assessment diagram analysis, here performed only for 316L, shows that the difference in trajectory is not very large and that this LME case should be considered as a special case of plastic collapse. This is related to the strain localization at the crack tip induced by the liquid metal. Further study of this phenomenon will be performed in the future. In view of the complicated fracture type shown by martensitic and austenitic type steels in contact with a heavy liquid metal, this type of analysis in terms of fracture mechanics could be interesting if applied to irradiated samples tested in liquid metals. In particular, a change of trajectory in the FAD for the unstable crack

growth would be an indication of possible synergistic effects between irradiation induced damage and LME. The FAD could then be an interesting mean for assessing cracks behavior in these very demanding conditions.

The overall conclusion of this investigation is that in spite of an embrittlement process taking place between the 316L austenitic steel with Hg and the martensitic steel T91 with PbBi, the degree of LME is sufficiently low to be considered as not relevant as a concern for mechanical design, in particular for spallation sources. This optimistic conclusion should not be extended however to irradiated materials where hardening and flow localization processes by irradiation defects could completely change the conclusion. We believe however, that fracture mechanics with the modifications of the type described in this work could be used to assess these potentially synergistic effects.

Acknowledgements

The authors would like to acknowledge the financial support from the FP6 European program IP-EUROTRANS (Contract No. FI6W-CT-2004-516520). Financial support from the French GDR GEDEPEON is also gratefully acknowledged.

References

[1] L.K. Mansur, J.R. Haines, J. Nucl. Mater. 356 (2006) 1.
[2] W. Wagner, Y. Dai, H. Glasbrenner, H.-U. Aebersold, J. Nucl. Mater. 361 (2007) 274.
[3] T. Auger, G. Lorang, Scripta Mater. 52 (2005) 6.
[4] L. Medina-Almazan, T. Auger, D. Gorse, J. Nucl. Mater. 376 (2008) 312.
[5] L. Medina-Almazan, J.C. Rouchaud, T. Auger, D. Gorse, J. Nucl. Mater. 375 (2008) 102.
[6] H. Tada, P.C. Paris, G.R. Irwin, The Stress Analysis of Cracks Handbook, Del Research Corporation, 1973.
[7] K.H. Schwalbe, B. Neale, Fatigue Fract. Eng. Mater. Struct. 18 (1995) 11.
[8] K.H. Schwalbe, A. Cornec, K. Baustian, Int. J. Pressure Vessel Piping 65 (1996) 193.
[9] Y. Lei, B.K. Neale, Fatigue Fract. Eng. Mater. Struct. 20 (1997) 15.
[10] J. Rensman, Specimen size effects in upper-shelf fracture toughness of F82H RAFM steel, NRG, 2003.
[11] I. Milne, Mater. Sci. Eng. 39 (1979) 14.